Methane Hydrate Crystallization Mechanism from *In-Situ* Particle Sizing

J. M. Herri
Ecole des Mines de Saint-Etienne, SPIN, 42023 Saint Etienne Cedex 2, France and
Institut Français du Pétrole, 92506 Rueil-Malmaison Cedex, France

J. S. Pic, F. Gruy, and M. Cournil
Ecole des Mines de Saint-Etienne, SPIN, 42023 Saint Etienne Cedex 2, France

A new experimental setup that makes possible in-situ determinations of the population density function of the methane hydrate particles during its crystallization in a pressurized reactor is used. Thanks to this equipment, new results can be obtained, in particular concerning the granular aspects of the crystallization processes and the influence of the stirring rate. These results are discussed in the framework of a model including gas absorption, primary and secondary nucleation, crystal growth, agglomeration, and breakage. From this discussion, the relevant processes and parameters of methane hydrate crystallization can be determined and quantified.

Introduction

Since their discovery in 1810 by Sir Humphrey Davy, interest in petroleum production for gas hydrate crystals has changed considerably (Sloan, 1990). These solid particles are obtained after the rearrangement of liquid water molecules around the dissolved gas molecules such as methane, ethane, and other hydrocarbon molecules that are usually present in the gas part of the petroleum fluid. To form, gas hydrates usually require high pressure (several tens of bard) and low temperatures (a few Celsius degrees), conditions that are commonly met in undersea pipelines (the greater the depth, the higher the pressure and the greater the ability of the crystals to form). To prevent the crystallization process, which can plug the valves and other transport facilities, one can inject additives such as methanol or glycols to eliminate the equilibrium temperature of formation from the operating conditions. These additives have a thermodynamic effect, and they are often used in large quantities (sometimes 50% in weight of the water phase). Moreover, because the amount of additives required increases with the pressure, such inhibitors cannot be used in the exploitation of the deepest wells.

Recently, new research tracks have been considered. Preference is now given to additives that can act as kinetic inhibitors of one or more of the crystallization processes. What makes this approach interesting is the small quantity of additives needed (about 1% in weight of the water phase). The efficiency of some of these additives has now been clearly proved. Validation experiments are generally performed on a circulating loop that simulates the transport of the petroleum fluid. The efficiency criteria are of different sorts: quantity of hydrate formed, pressure drop in the pipes, induction period and subcooling required for a rapid crystallization. The nature of the additive effect is rarely well understood, however, mostly because of the lack of experimental results concerning the nucleation growth of the hydrate phase.

Several mechanisms of gas hydrate crystallization have been proposed. Most of them are relative to an experimental simplified system consisting of pure water and a gaseous hydrocarbon, generally methane. At zero time, the gaseous hydrocarbon is fed into the batch or semibatch reactor, which initially contains pure liquid water. During crystallization, the quantity of the gas that is incorporated in the solid hydrate phase is monitored. In the earliest models, gas hydrate crystallization was modeled from the only information concerning the quantity of gas absorbed. The gas/liquid interface was soon identified as a critical zone due to the high level of methane concentration. Bishnoi and coworkers (Vysniauskas and Bishnoi, 1983, 1985; Englezos et al., 1987a,b) have observed that the first crystals generally appear in the film region just beneath the gas/liquid interface and then disperse in the bulk. This observation has been reported by most of the research teams working on the gas hydrate crystallization.

Correspondence concerning this article should be addressed to M. Cournil.

This behavior was equally visually observed in another system in which one of the reactants is supplied through the gas/liquid interface (Washi and Jones, 1991a,b). The importance of the gas/liquid interface was considered in the first microscopic approach proposed by Bishnoi and coworkers (Vysniauskas and Bishnoi, 1983, 1985). In a thin interfacial film, concentration in dissolved gas varies from the solubility value (imposed by gas pressure) to the bulk value. Using a population balance model, which takes into account primary and secondary nucleation and growth, these authors proposed a correlation between crystal growth rate and gas consumption rate; they identified growth as the rate-determining step of crystallization. This conclusion was recently contradicted by Skovborg and Rasmussen (1994). Using the experimental results of Bishnoi and coworkers, they proposed a simplified model in which the limiting step is the mass transport of gas in the film region rather than one of the crystallization processes. This conclusion was confirmed by Gaillard (1996) and Herri (1996). This implies that the population density function of the particles is not accessible from measurements of gas consumption, whereas it is clear that the kinetic models of gas hydrate formation should be based on crystallization models using the population balance equation (Randolph, 1964; Vysniauskas and Bishnoi, 1983; Randolph and Larson, 1988). As pointed out by the results of Skovborg and Rasmussen (1994), however, validation of the gas hydrate crystallization models requires data concerning the crystal size.

In a more general way, in powder technology and in industrial crystallization, determination of particle-size distribution (PSD) during a process is of major interest for practical reasons of control or monitoring as well as for the fundamental understanding of the observed phenomena. Among the numerous methods of particle sizing, the least intrusive are the optical methods. Montfort and Nzihou (1993) and Bylov and Rasmussen (1997) applied such methods to the in-line characterization of gas hydrate PSD. Our research group has developed a turbidity sensor, which is compatible with *in-situ* PSD determinations (Crawley et al., 1997). This technology has been successfully applied to the characterization of the methane hydrate crystallization in a semibatch reactor (Herri, 1996).

This article is organized as follows: in the first part we recall the physical and mathematical principles of turbidimetry used as a particle-sizing method; the second part is first devoted to the description of our experimental setup, and then to the main results obtained relative to the crystallization of methane hydrate. In the third part, titled ''Theory,'' these results are discussed in the framework of a model in order to derive conclusions concerning the mechanism of the methane hydrate crystallization. This model takes the crucial importance of the rate-determining mass transfer at the gas/liquid interface, as pointed by Skovborg and Rasmussen (1994), into account.

Particle-Size Determination from Turbidity Data in the Particular Case of Methane Hydrate

Turbidity

When a parallel light beam of wavelength λ is crossing a suspension, the different scattering effects caused by encounters with solid particles result in a global extinction phenomenon, from which the turbidity τ_λ definition comes:

$$\tau_\lambda = \frac{1}{L} \log \frac{I_0}{I_L}, \tag{1}$$

where I_0 is the intensity of the incident ray and I_L is the intensity of the transmitted ray after an optical path length L. According to van de Hulst (1957) and Kerker (1969), the turbidity spectrum of a suspension of spherical nonabsorbent grains is linked to its PSD by the following relation:

$$\tau_\lambda = \frac{\pi}{4} \int_0^\infty Q_{\text{sca}}(\lambda, D, m) D^2 f(D)\, dD, \tag{2}$$

where $f(D)$ is the population density function of the particles with diameter D. The scattering coefficient Q_{sca} of a particle is dependent on the wavelength λ of the incident ray and on the ratio m between the refractive indices of the particle and of the liquid medium.

It is theoretically possible to calculate the PSD $f(D)$ of a suspension from its turbidity spectrum using Eq. 2 (Eliçabe and Garcia Rubio, 1989; Crawley et al., 1997). This requires several steps that were discussed in an earlier article by Herri and coworkers (1998). For methane hydrate crystals suspended in water, only the range [10 μm to 150 μm] is wholly accessible from these calculations. Moreover, the turbidity data can be used only for turbidity values lower than about 2. This restricts the use of turbidimetry to dilute suspensions (about 10^{-2}–10^{-3} in solid volume fraction).

Experimental Part

Experimental setup

The experimental setup used in this study was especially designed to keep the temperature and pressure constant throughout an experiment, to measure the consumption of methane absorbed by the liquid solution during hydrate crystallization, and to acquire the turbidity spectrum of the suspension of methane hydrate particles by in-line measurements.

The reactor cell is a Pyrex cylinder. It is filled with 800 cm^3 to 1,200 cm^3 deionized water. The cell is located in a stainless-steel autoclave, in which the pressure can be raised to 120 bar. The autoclave is surrounded by a cooling jacket through which glycol is circulated from a cryostatic temperature controller. Two sapphire windows mounted one on each side of the reactor make possible the observation of crystal crystallization or dissociation. During the hydrate crystallization, pressure control is achieved by measuring the differential pressure ΔP between the reactor and a ballast pressure reference. The suspension is stirred by a four vertical-blade turbine impeller whose rotation rate can be varied between 0 and 600 rpm.

Temperature is monitored by a platinum thermocouple. The turbidimetric sensor is a UV–visible analyzer that measures *in-situ* the attenuation of a polychromatic beam in the wavelength range (230 nm, 750 nm). We have developed an in-line acquisition system consisting of: (1) a polychromatic

xenon arc lamp; (2) two fiber optics (one leads light from the arc lamp to the *in-situ* sensor; the other one leads the transmitted light from the sensor to a commercial fiber optics spectrophotometer); (3) and a sensor especially designed for this application. This sensor is composed of two identical elements: the first one generates a parallel light beam, and the second one acts as a collimator. The optical path between the two elements is usually one centimeter. A more detailed description of this setup can be found in (Herri et al., 1998).

Experimental results

The experiments reported here were planned to improve the understanding of the mechanism of crystallization of methane hydrate.

(1) Methane Dissolution in Water. The aim of these experiments was to determine the kinetics of the mass-transfer step corresponding to the dissolution of methane in water. To achieve this, we chose the operating conditions so that gas absorption would be over before the appearance of the first crystals. At time zero, the methane pressure is suddenly raised from 1 to 55 bar; temperature is set at 1°C. Gas consumption is recorded for different stirring rates throughout the dissolution process. In all cases, a first-order law is found that is quite consistent with the well-known relation (Mehta and Sharma, 1971; Sridharan and Sharma, 1976):

$$r = k_L a(C_{\text{ext}} - C_b), \tag{3}$$

where r is the dissolution rate per unit volume ($\text{mol}\cdot\text{cm}^{-3}\cdot\text{s}^{-1}$); a is the mass-transfer surface area per volume of liquid (cm^{-1}) and k_L is the mass-transfer coefficient ($\text{cm}\cdot\text{s}^{-1}$); C_b is the methane concentration in the bulk of the liquid; and C_{ext} is the interfacial concentration imposed by the gas/liquid equilibrium.

Figure 1 gives the variation of $k_L a$ with the stirring rate ω (expressed in rpm).

(2) Primary Nucleation from an Aqueous Methane Solution. When the methane/water system is brought into the thermodynamic conditions of the hydrate crystallization, the appearance of the first crystals is generally not immediate, but occurs after an induction period. In the experiments reported here, the starting point is located in the dissociation zone ($T = 20$°C and $P = 20$ to 30 bar). The solution is then cooled very slowly to a temperature value equal to the operating temperature (here 1°C). Then the pressure is suddenly raised to its operating value P_K. Thus the system is brought into the crystallization area within a few tens seconds; this way, a supersaturation level $S = P_K/P_J$ is reached (P_J is the equilibrium pressure at 1°C). This procedure is expected to initiate a primary nucleation process within a solution that is supposed to contain no associated solute molecules. By varying P_K, it is possible to study the effect of the supersaturation level S on the induction period t_L (Figure 2). The figure also shows the good agreement between the experimental points and the classic law (dotted line):

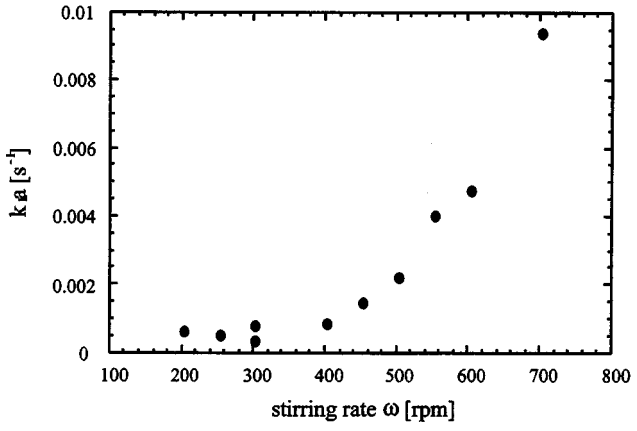

Figure 1. Influence of the stirring rate on the rate of methane absorption.

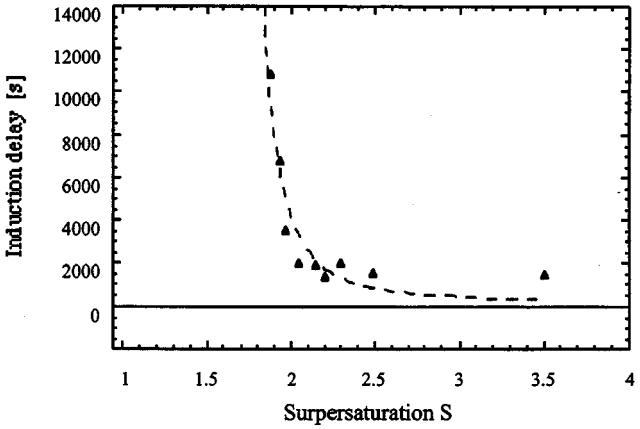

Figure 2. Influence of supersaturation (i.e., pressure) on the induction period during crystallization of methane hydrate at a temperature of 1°C and a stirring rate of 400 rpm.

$$t_L \approx \exp\left(\frac{B}{\log^2(S)}\right)$$

in which B is a constant (Zettlemoyer, 1969).

(3) Influence of the Stirring Rate on the Flotation of the Particles. The density of the methane hydrate particles (910 $\text{kg}\cdot\text{m}^{-3}$) is less than water. Visually, one can see that a noticeable amount of the hydrate particles is located near the gas/liquid interface, and so is not detected by the turbidimetric sensor, which is located in the bulk zone. In order to quantify the percentage of particles in the bulk zone compared to the total quantity of particles, we have calculated the ratio q between:

- The particle volume $V_{p\text{Turb}}$ calculated using the turbidity signal (Figure 3);
- The bulk particle volume $V_{p\text{GPIB}}$ calculated from the total volume of methane gas that has been incorporated into the liquid phase during the crystallization (Figure 3).

Figure 3 shows ratio q vs. time for an experiment that was performed at a stirring rate of 400 rpm, a pressure of 35 bar, and a temperature of 1°C. We can observe that ratio q remains constant during all the experiment, and so is not dependent upon the quantity of hydrate formed.

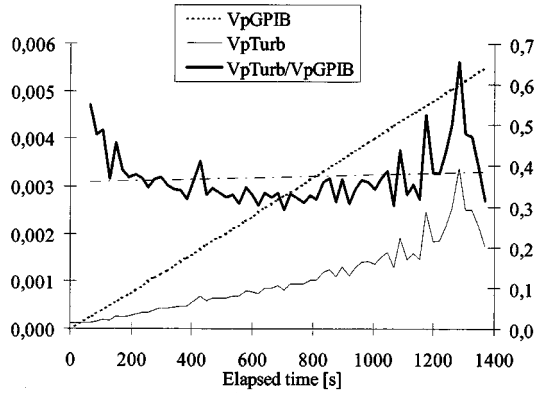

Figure 3. Experimental V_{pGPIB} and V_{pTurb} values and ratio $q = V_{pTurb} / V_{pGPIB}$.

Table 1 shows the values of q at different stirring rates (200, 300, 400 and 500 rpm) and different pressures (35 and 45 bar). We can see that q does not vary with the pressure and, more surprisingly, is not significantly dependent upon the stirring rate, at least within the reproducibility range.

So, whatever the pressure and stirring rate conditions, the ratio between the floating particles and the bulk particles seems to remain constant, or at least varies little and stays within the range between 0.3 and 0.5. Nevertheless, problems of irreproducibility between the different experiments cannot be avoided. This point is discussed later.

(4) Influence of the Stirring Rate on the Crystals Sizes. The experiments reported here are carried out at low supersaturation (experimental pressure of 31 bar and equilibrium pressure of 29 bar at $T = 1$°C), so that crystallization is not too rapid and turbidity data can be exploited. However, the fact that the driving force of the process is relatively small is a cause of irreproducibility. This difficulty generally has been overcome by adopting a rigorous procedure of thermal preparation of the system (Herri, 1998) that considerably enhances the reproducibility of the results, and more particularly the induction time.

Figure 4 gives an example of the data that are directly available from each experiment, that is, turbidity vs. time at different wavelengths (Figure 4a) and methane consumption vs. time (Figure 4b). The time evolution of the PSD (Figure 5a), the global volume fraction of hydrate particles (V_{PGPIB} solid line in Figure 5b), and the part of this volume fraction accessible to our sensor (V_{PTurb}; dashed line in Figure 5b) can be calculated from these results.

The influence of the stirring rate is shown in Figure 6 on the mean particle diameter (Figure 6a) and total number (Figure 6b), respectively. The evolution with time of the mean

Table 1. Experimental q Value as a Function of the Pressure and of the Stirring Rate

	ω [rpm]			
P [bar]	200	300	400	500
35	0.5	0.3–0.6	0.4	0.3–0.5
45	0.5	0.3–0.5	0.5	—

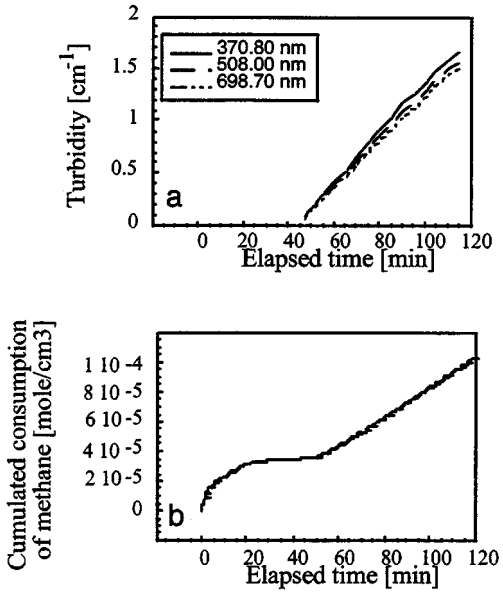

Figure 4. Experimental data: turbidity vs. time (a) and consumption of methane (b).

diameter and of the total number of particles is also widely dependent on the stirring rate. At a low stirring rate (250 rpm), the average diameter increases with time, while it maintains constant values at an intermediate stirring rate (400 rpm), and decreases again at high a stirring rate (600 rpm). Where the total number of particles is concerned, the time evolution is very different according to the stirring rate. In fact, at the lowest stirring rate (250 rpm), the total number of particles increases less and less quickly. On the other hand, it

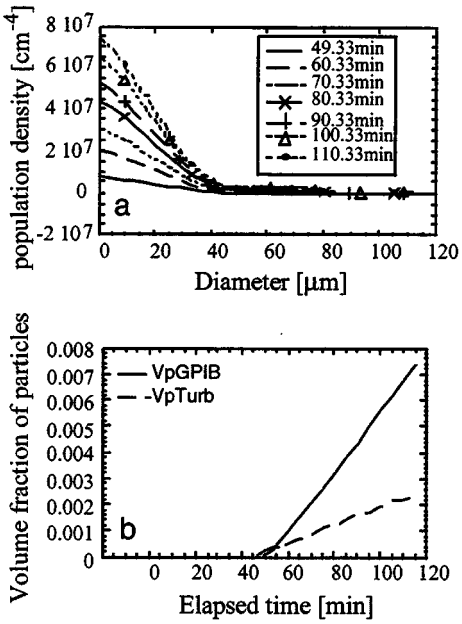

Figure 5. Calculated data: population density function (a) and volume fraction of particles (b).

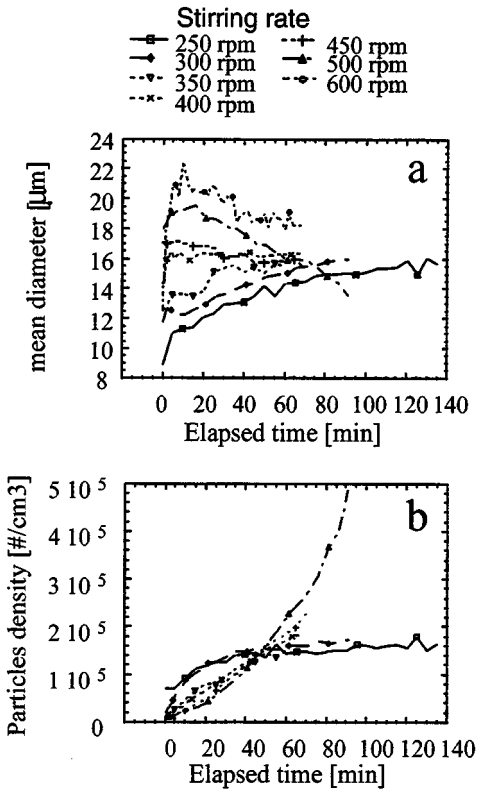

Figure 6. Influence of the stirring rate on the mean diameter (a) and on the number of particles (b) during the crystallization of methane hydrate at 30 bars and 1°C.

increases more and more rapidly at the highest stirring rates (500 rpm). For intermediate values, the total number of particles increases at a constant rate.

From these results we can expect the stirring rate to have a complex effect on the size, the number of particles, and the absorption of methane. Understanding these behaviors requires a model for each process: absorption, nucleation, growth, and agglomeration, particularly in order to calculate a theoretical PSD and to compare it with the experimental PSD.

About the performances of the method

The conditions of using our turbidimetric method are closely dependent on the validity of Eq. 2. This results in restrictions on

- Volume fraction of particles that must be inferior to 0.01
- Diameter of particles that must range from 10 to 150 μm.

We have observed experimentally that the volume fraction of the hydrate phase rarely exceeds 0.01, or reaches this value after a lengthy experiment. Moreover, the mean diameter values calculated here are always in the diameter range [10–22 μm]. So, we can consider that the turbidimetric technique is particularly well adapted to the study of the crystallization of the methane hydrate particles.

The experimental results have shown excellent reproducibility for the mean diameter calculated using the turbidimetric signal, but not for the total number of particles and the total volume of particles $V_{p\mathrm{Turb}}$. On the other hand, we have observed good reproducibility for the results deduced from the quantity of methane absorbed during the crystallization, that is, good reproducibility of the methane consumption rate and of the total volume of particles $V_{p\mathrm{GPIB}}$.

Thus, the origin of the average reproducibility of ratio $q = V_{p_{\mathrm{Turb}}}/V_{p_{\mathrm{GPIB}}}$ lies in the relative dispersion of the $V_{p\mathrm{Turb}}$ measurements; consequently, this error causes dispersion of the total number of calculated particles. At the moment we have no procedures for determining the origin of this dispersion.

So, the validity of the models (which are presented now) will be understood according to their ability to predict correct diameter values, while moderate errors in the particle number will be accepted.

Theory

Our model can be broken down into the following two parts:

(a) Mass and population balances in which we list all the mechanisms that we have envisaged.

(b) Model of the complex effect of the stirring rate on the PSD. For this, we base our discussion on the experimental results concerning: the effect of the stirring rate on the initial number of particles and their diameter; the effect of the stirring rate on the evolution of the particle number and diameter with respect to time.

(a) Mass and Population Balances. Two zones can be distinguished in the stirred reactor (Figure 7) as pointed by Vysniauskas and Bishnoi (1983) and Jones and coworkers (1992):

- The first zone is the interface layer; in the system investigated, its thickness is about a few tens of micrometers. Because of this small value, the concentration gradient in dissolved methane should be constant, and among the different crystallization processes, only primary nucleation is envisaged. Because of the high supersaturation level of this zone compared to the rest of the reactor, primary nucleation is

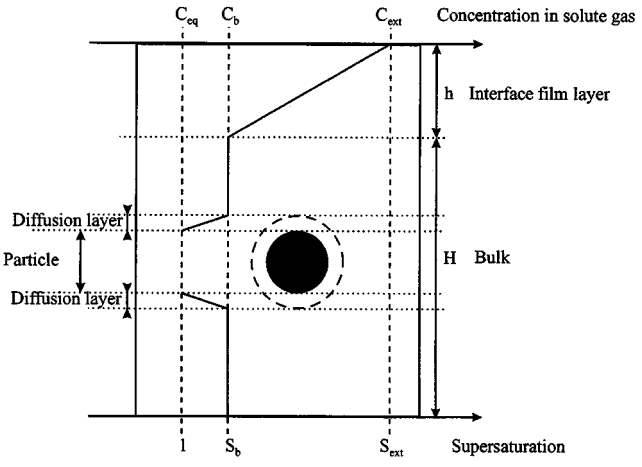

Figure 7. Concentration profiles in the reactor.

particularly active in the interfacial film, which acts most of the time as a source of nuclei for the bulk of the reactor. Thus, unlike other authors [Jones and coworkers (1992)], we will not write the population balance equation in the interfacial film, which is useless in our case.

• The second zone is the bulk zone, in which the concentration should be uniform. This zone should be the main place for the crystallization process, in which we can find all the classic steps of primary nucleation—growth, agglomeration, and secondary nucleation. The area of the liquid/gas interface is assumed to be independent of time. However, floating hydrate particles could reduce the interfacial area available for methane absorption. This has not been considered here, because in our experimental conditions, only a small quantity of hydrates is formed and this amount probably does not perturb absorption. This is also confirmed by the constant rate of gas consumption during the first two hours of the experiments.

The main variables of the system are the population density function in the bulk zone $f(R, t)$, and the concentration $C_b(t)$ in dissolved methane in the bulk zone; t denotes the time and R the equivalent particle radius.

Two equations can be written to represent the time evolution of the system:

(1) The population balance equation of the hydrate crystals (Randolph, 1964)

$$\frac{\partial f}{\partial t} + G\frac{\partial f}{\partial R} = B'(R) - D'(R). \qquad (4)$$

In this expression, it has been assumed that the growth rate $G(G = (dR/dt))$ is independent of the grain size.

The "birth" term $B'(R)$ is due to the contributions of primary nucleation, secondary nucleation, breakage, and agglomeration. The "death" term $D'(R)$ is essentially due to agglomeration.

(2) The mass balance equation in dissolved methane in the bulk zone:

$$\frac{dC_b}{dt} = k_L a\cdot(C_{\text{ext}} - C_b) - \frac{4\cdot\pi}{v_m}\cdot GM_2, \qquad (5)$$

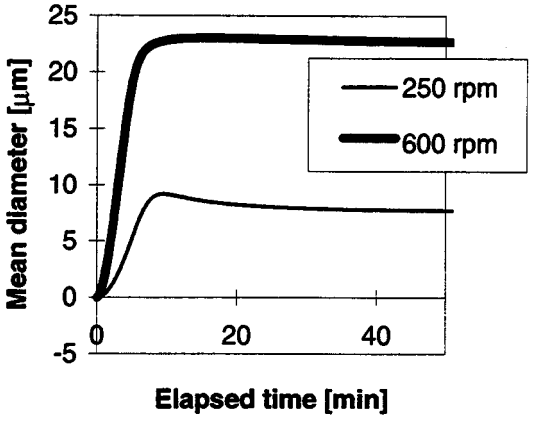

Figure 8. Simulation of the mean diameter in a simplified model of primary nucleation/growth.

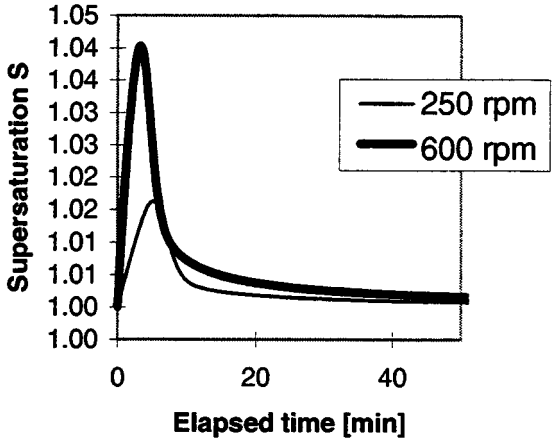

Figure 9. Simulation of the supersaturation in a simplified model of primary nucleation/growth.

where v_m is the molar volume of the hydrate particles; and M_2 is the second moment of the population density function.

(b) Interpretation of the Effect of the Stirring Rate on the Initial Particle Number and Mean Diameter of Particles. Experimental results (Figures 6a and b) show that the initial mean diameter—the mean diameter value of the crystal population just after the initial sharp increase that can be seen both on the experimental and simulated plots (Figures 6a, 8, 10, 12 and 14)—increases as the stirring rate increases. At a stirring rate of 250 rpm, its value is about 10 μm, while it is about 20 μm at a stirring rate of 600 rpm. On the other hand, the initial total number of particles decreases with increasing stirring rate.

To explain such behavior, we have based our model on the description proposed by Jones and coworkers (1992) in a problem similar to ours, that is, precipitation of calcium carbonate in a small flat interface gas/liquid reaction cell via the gaseous carbonation of lime water. In fact, these authors have observed a similar experimental effect of the stirring rate, that is, an increase in the mean crystal size with increasing stirring rate and a simultaneous decrease in the total

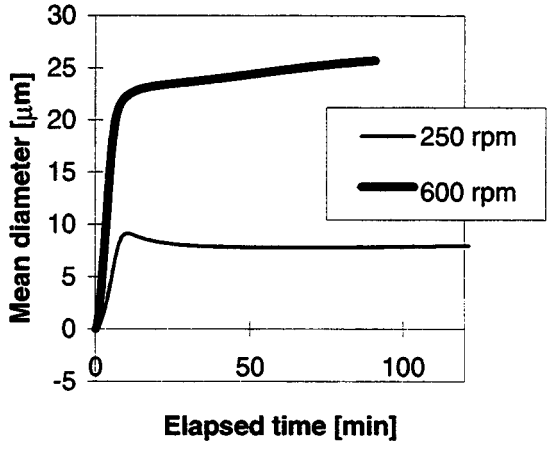

Figure 10. Simulation of the mean diameter in the presence of agglomeration.

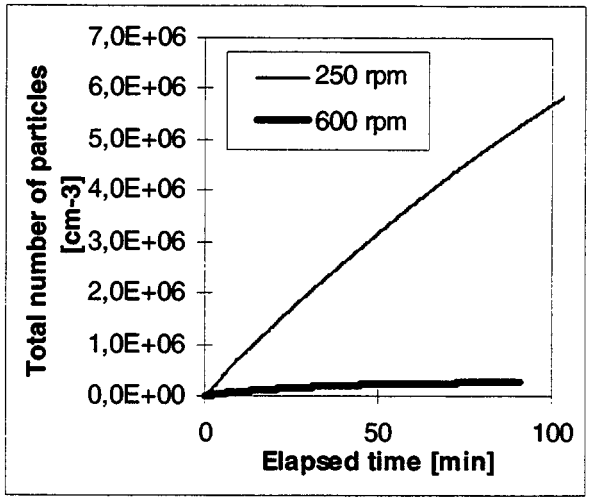

Figure 11. Simulation of the total number of particles in the presence of agglomeration.

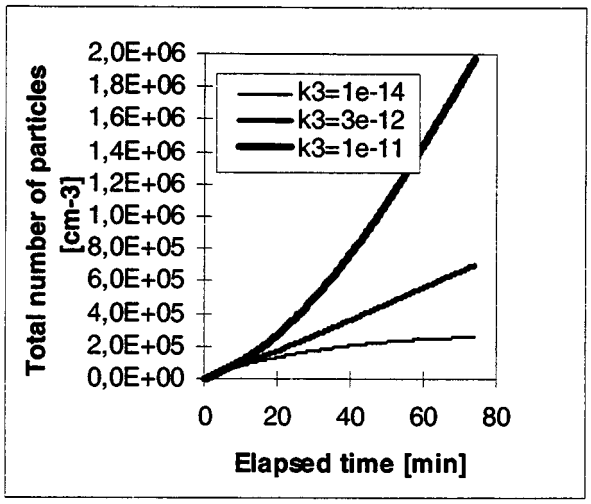

Figure 13. Influence of k_3 (attrition constant) on the total number of particles at a stirring rate of 600 rpm.

number of particles. In their approach, the film region is a zone of primary nucleation due to the high level of concentration of dissolved gas. This analysis is quite different from that proposed by Bishnoi and coworkers (Vysniauskas and Bishnoi, 1983, 1985), who assumed that primary nucleation occurs only at the start of crystallization, and then is inactive. Then, the nuclei size can be calculated using the Volmer theory (Volmer and Weber, 1926), their number is assumed to be constant because they "instantaneously" consume the excess gas dissolved in the solution, thus preventing further nucleation. In the approach of Jones and coworkers, primary nucleation takes place in the film region and is never inactive, but instead is a continuous source of nuclei. Moreover, the thickness of his film region depends on the stirring rate and is equal to

$$h = \frac{\mathfrak{D}}{k_L}, \tag{6}$$

where $\mathfrak{D}$ is the diffusivity of the gas molecules in the liquid water.

From the experiments reported earlier (Figure 1), it appears that $k_L a$ strongly increases with the stirring rate. Since the a variation is limited (visual observation), we can conclude that, as the stirring rate increases, the film thickness decreases. Because, on the other hand, primary nucleation is active mostly in the interfacial zone, the global production of nuclei per unit of time decreases too; these fewer nuclei, which are then submitted to the same excess in dissolved gas, can grow to larger sizes. This is indeed the behavior observed in our experiment.

To quantify this effect exactly, we have to include it in a model. The first step is to adopt a quantitative description of all the processes considered:

(1) Methane absorption (correctly described by Eq. 3);

(2) Primary nucleation. From the nucleation experiments reported in Figure 2, we keep the validity of the classic ex-

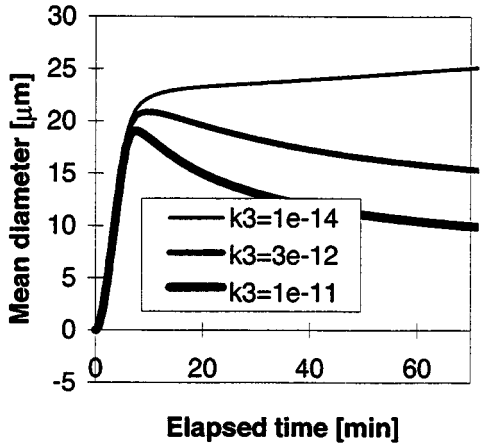

Figure 12. Influence of k_3 (attrition constant) on the mean diameter at a stirring rate of 600 rpm.

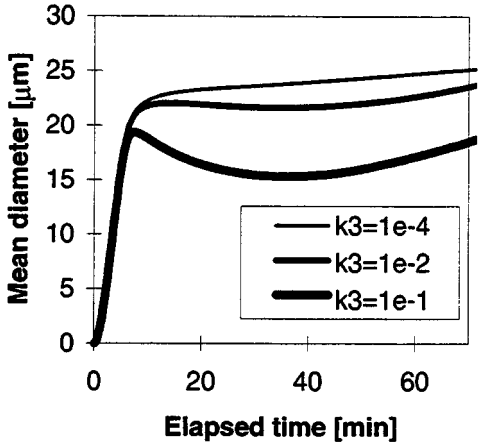

Figure 14. Influence of k_3 (breakage constant) on the mean diameter at a stirring rate of 600 rpm.

pression of the nucleation rate B_I (i.e., the number of nuclei produced per unit volume and unit time):

$$B_I(C_b) = k_1 \exp\left(-\frac{B}{\log^2 S}\right) \quad \text{with} \quad S = \frac{C_b}{C_{\text{eq}}}, \quad (7)$$

in which k_1 and B are constant. We want to keep the form of Eq. 7, to estimate parameters k_1 and B (as explained further in this text). We assume that the gradient concentration in dissolved methane (i.e., of supersaturation), which results from the low thickness of the film region, is constant. The rate of primary nucleation in the film region can be expressed as

$$B_{I,1} = k_1 h \frac{S}{V} \int_0^h \exp\left(-\frac{B}{\log^2 S(x)}\right) dx \quad \text{with}$$

$$S(x) = S_{\text{ext}} + \frac{S_b - S_{\text{ext}}}{h} x. \quad (8)$$

The concentration in solute methane (thus, the supersaturation) in the bulk zone should be uniform, and then the rate of primary nucleation can be expressed as

$$B_{I,2} = k_1 \exp\left(-\frac{B}{\log^2 S_b}\right). \quad (9)$$

(3) Crystal growth. Following the example of Englezos et al. (1987a, b) and Skovborg and Rasmussen (1994), we propose to take the particle growth rate in the form

$$G = k_g(C_b - C_{\text{eq}}), \quad (10)$$

where C_{eq} is the equilibrium concentration in dissolved methane in the presence of the hydrate phase, and C_b is the bulk concentration. The growth rate constant k_g should include the following consecutive steps:

- Gas transport from the bulk of the solution to the liquid/crystal interface;
- Incorporation of gas molecules into the hydrate structure.

Because of the strong and complex dependence of the mean particle radius on the stirring rate, as shown in our experiments, we assume that the second step, insensitive to hydrodynamic effects, is not the rate-determining step, and we propose expressing k_g using correlations frequently met in mass-transport phenomena.

The correlation of Armenante and Kirwan (1989) gives the following relation between the Sherwood number Sh_p and the Reynolds number Re_p of the particles and the Schmidt number Sc:

$$Sh_p = 2 + 0.52\, Re_p^{0.52} Sc^{1/3} \quad (11)$$

with

$$Sh_p = \frac{k_d \cdot D}{\mathfrak{D}}, \qquad Sc = \frac{\upsilon}{\mathfrak{D}}, \qquad \text{and} \qquad Re_p = \frac{D^{4/3}\epsilon^{1/3}}{\upsilon},$$

where

$\mathfrak{D} = 9.67 \times 10^{-5}$ m$^2 \cdot$s^{-1} is the diffusivity of methane in water (Wilke and Chang, 1955)
$\upsilon_m = 1.3 \times 10^{-4}$ m$^3 \cdot$mol^{-1}
$\upsilon = 1.79 \times 10^{-6}$ m$^2 \cdot$s^{-1} is the kinematic viscosity of water at 0°C
ϵ is the energy dissipation rate per unit mass of fluid, and is given by

$$\epsilon = \frac{N_p D_S^5 N^3}{V} \qquad \text{(Baldi et al., 1978);} \quad (12)$$

$V = 10^{-3}$ m^3 is the volume of the stirred medium
$D_S = 0.058$ m is the stirrer diameter
$N =$ stirring rate (in round per second)

N_p is the power number of the stirring device, and is near 1 (four vertical blade stirrer).

Armenante and Kirwan's conditions of validity correlation ($D < 30$ μm, $Re_p > 10^{-2}$, and $Sh_p > 3.5$) are globally satisfied in our system. Thus, the relation between k_g, ω (stirring rate in rpm), and D is

$$k_g = 2.54 \times 10^{-13}\, D^{-1} + 2.5423 \times 10^{-11} \cdot D^{-0.31} \omega^{0.52}, \quad (13)$$

where k_g is in m$^4 \cdot$mol$^{-1} \cdot$s^{-1}, and D is in m.

To keep a non-size-dependent growth rate in the calculations, we replace k_g by an averaged value $\tilde{k}_g$ over the experimental size interval, to obtain

$$\tilde{k}_g = 1.2 + 0.06\, \omega^{0.52} \text{ cm}^4 \cdot \text{mol}^{-1} \cdot \text{s}^{-1}, \quad (14)$$

with ω in rpm. These first elements now can be integrated into a simplified model in which only primary nucleation and growth are envisaged.

Simplified crystallization model

The simulation presented here takes into account the kinetics laws (Eq. 3) for methane absorption, (Eqs. 8 and 9) for primary nucleation, and (Eqs. 10 and 14) for crystal growth. The equation set to be solved consists of Eq. 5 (mass balance in dissolved methane) and Eq. 4 (population balance):

$$\frac{\partial f}{\partial t} + G \frac{\partial f}{\partial R} = (B_{I,1} + B_{I,2}) \delta(R), \quad (15)$$

where $\delta(R)$ is the Dirac function (it is assumed that new particles created by primary nucleation have an initial size of zero). The initial conditions are $f(R, t = 0) = 0$ and $C_b(t = 0) = 0$.

Solving the model

The method of the moments has been applied to solve the problem. The jth-order moment of the PSD is defined as

$$M_j = \int_0^\infty R^j \cdot f(R)\, dR. \quad (16)$$

Thus, the population balance equation (Eq. 15) can be transformed in the ordinary differential equations system:

$$\frac{dM_0}{dt} = B_I \quad \text{and} \quad \frac{dM_j}{dt} = j \cdot G \cdot M_{j-1} \quad \text{for} \quad 1 \le j \le 6$$

For $j \ge 6$, the system is closed by the relation, $M_j = \bar{R}^{j-5} M_5$:

$$\frac{dC_b}{dt} = k_L a \cdot (C_{\text{ext}} - C_b) - \frac{4 \cdot \pi}{v_m} \cdot G M_2$$

The system is solved by the Runge-Kutta method. In this article, we present only the relative supersaturation of the liquid phase, $S_b = C_b(t)/C_{\text{eq}}$, the total number of particles per unit volume, $N_T = M_0$, and the particle mean radius $\bar{R} = M_1/M_0$.

In fact, these results can be derived from the solution of the first four equations (in M_0, M_1, M_2, M_3, M_4) and of the equation in C_b.

Simulation results

Figure 8 shows the model prediction of the early stages of crystallization. One can see that the behavior of the initial mean diameter and supersaturation with respect to the stirring rate is in agreement with the observed trends. The initial mean diameter increases from 10 μm to 20 μm as the stirring rate increases from 250 rpm to 600 rpm. Results that are not presented here show that the initial total number of particles decreases as the stirring rate is increased, as in the experimental results. In this primary nucleation/growth model, the constants k_1 and B, are the fitting parameters which quantify the primary nucleation. The initial average diameter is accurately determined, and the effect of the stirring rate properly simulated using the right couple (k_1, B). It also can be noted that an infinity of couples (k_1, B) give exactly the same results, for instance ($k_1 = 3 \times 10^{95}$ cm$^{-4} \cdot$s^{-1}; $B = 1$) and ($k_1 = 2 \times 10^3$ cm$^{-4} \cdot$s^{-1}; $B = 0.01$), because they correspond to the same flux of primary nucleation. A parametric study of the pressure effect could allow us to determine the actual values of k_1 and B.

Figure 9 shows the evolution of the supersaturation in the bulk zone. First, dissolving the methane gas in the liquid solution via the gas/liquid interface causes it to increase. When the supersaturation reaches value 1, the primary nuclei, which are formed at the interface, can pass into the bulk zone and begin to grow. The consumption rate due to the crystal growth is poor, however, due to the small quantity of particles and the low value of the growth driving force ($C_b - C_{\text{eq}}$). The supersaturation therefore continues to increase and reaches a maximum. At this moment, the rate of absorption of methane is equal to the consumption rate due to growth. After that, the growth consumption rate becomes higher than the absorption rate and the supersaturation decreases.

Advanced crystallization model

In the previous subsection, we showed that a model of primary nucleation/growth is sufficient to describe the early stage of crystallization and the influence of the stirring rate on the initial mean diameter. Now, we have to explain the influence of the stirring rate on the mean diameter and total number of particles throughout the crystallization process.

The experimental results show:

- At a low stirring rate of 250 rpm, the mean diameter increases with respect to time and the total number of particles increases less and less quickly.
- At a high stirring rate of 600 rpm, the mean diameter decreases with respect to time and the total number of particles increases more and more quickly.

In order to explain such a complex effect of the stirring rate, we have to consider processes other than primary nucleation and growth. We will show that agglomeration and breakage must be included in the simulation. To quantify their effects, we will introduce them successively into the model, beginning with agglomeration, then going on with breakage.

Agglomeration. At a low stirring rate of 250 rpm, the experimental mean diameter increases with respect to time, and the total number of particles increases less and less quickly. Using a simple model of primary nucleation/growth, the simulations give a total number of particles that increases continuously vs. time, whereas the mean diameter remains constant.

A good way to interpret the experimental observations is to use agglomeration in the simulation, because its qualitative effect is to increase the mean diameter and to decrease the total number of particles.

The contribution of agglomeration to the population balance equation is expressed by the term A_g (von Smoluchovski, 1917; Randolph and Larson, 1988):

$$A_g = \frac{1}{2} \int_0^v K(v - v', v') \cdot f'(v - v') \cdot f'(v')\, dv' - f(v) \cdot \int_0^\infty K(v, v') \cdot f'(v')\, dv' \quad (17)$$

where v and v' are particle volumes; f' is the population density function by volume v; and $K(v_i, v_j)$ is the agglomeration kernel between two particles of volume v_i and v_j. Several models express $K(v_i, v_j)$ as a function of the particle sizes and the hydrodynamic conditions of the medium. In the range of stirring rates investigated here, we consider the models of turbulent agglomeration (Camp and Stein, 1943; Saffman and Turner, 1956; De Boer et al., 1989); these models are characterized by the following expression of the kernel:

$$K_{i,j} = \frac{4}{3} \dot{\gamma} \alpha (r_i + r_j)^3 \quad (18)$$

where $\dot{\gamma} = \sqrt{\frac{2}{15} \frac{\epsilon}{\nu}}$ is the velocity gradient in a Kolmogorov eddy; r_i, r_j are the respective radii of the agglomerating particles; and α is the capture efficiency coefficient (van de Ven and Mason, 1977; Higashitani et al., 1982, 1983).

We propose to simplify this expression by writing

$$K^0_{i,j} = \frac{4}{3} \alpha \dot{\gamma} (2\bar{R})^3 \quad (19)$$

where $\bar{R} = (M_1/M_0)$ (M_1 and M_0 are, respectively, the first-order and zero-order moments of the PSD and $\bar{R}$ is the mean radius).

In order to consider the efficiency factor of the collision α, one obtains

$$K = 1{,}3\alpha\dot{\gamma}(2\bar{R})^3 \tag{20}$$

To estimate coefficient α, we have used the Higashitani et al. (1982, 1983) approach, in which α can be expressed by the relation

$$\alpha = C_A^{0.18} \qquad \text{with} \qquad C_A = \frac{A}{36\pi\mu\dot{\gamma}\bar{R}^3} \tag{21}$$

Since no data concerning A (Hamaker constant of methane hydrate in water) are available in the literature, we calculated it from the Gregory (1969) procedure. Here, A is obtained from the refractive indices of water and methane hydrate. More precisely, we need to know the wavelength dependence of both of them. Data concerning water are easily found in the literature (Gregory, 1969). In an earlier article, we derived the data relative to methane hydrate from the Lorentz—Lorenz model (Herri and Gruy, 1995); these data have been experimentally confirmed by Bylov and Rasmussen (1997). For a mean diameter equal to 10 μm, α is found equal to about 3×10^{-4}. This extremely low value is due to the structural similarity between water and methane hydrate.

Solving the model

The method of the moments is applied to solve the problem. The population balance equation (Eq. 5) therefore can be transformed in adding the terms of agglomeration in the previous expression of the moments:

$$\frac{dM_0}{dt} = B_I + A_0 \qquad \text{and} \qquad \frac{dM_j}{dt} = j\cdot G\cdot M_{j-1} + A_j,$$

$$\text{for} \quad 1 \le j \le 6$$

The system is closed for $j \ge 6$ by the relation $M_j = \bar{R}^{j-5}M_5$.

A_j is the contribution of A_g to (dM_j/dt). It is expressed as $A_j = \int_0^\infty R^j \cdot Ag\ dR$; $A_0 = -(K/2)M_0^2$, $A_3 = 0$, and $A_6 = K\cdot M_3^2$. Calculation of the other A_j values ($j = 1, 2, 4, 5$) requires an approximation of $f'(v)$ [or equivalently of $f(R)$]. For this, we consider the form of $f(R)$, derived from the experimental results (Figure 5a), that is,

$$f(R) \cong K_A\left[1 - \frac{R}{K_B}\right] \tag{22}$$

where K_A and K_B do not depend on R. The unknown terms A_j can then be estimated. Hence, the differential system

$$\frac{dM_0}{dt} = B_I - \frac{K}{2}M_0^2$$

$$\frac{dM_1}{dt} = GM_0 - 0.262\,KM_1M_0$$

$$\frac{dM_2}{dt} = 2GM_1 - 0.113\,KM_2M_0$$

$$\frac{dM_3}{dt} = 3GM_2$$

$$\frac{dM_4}{dt} = 4GM_3 + 0.097\,KM_4M_0$$

$$\frac{dM_5}{dt} = 5GM_4 + 0.188\,KM_5M_0$$

$$\frac{dM_6}{dt} = 6GM_5 + KM_3^2$$

$$\frac{dC}{dt} = k_La(C_{\text{ext}} - C) - \frac{4\cdot\pi}{v_m}GM_2 \tag{23}$$

Simulation results

Figure 10 shows the simulated mean diameter vs. elapsed time at two stirring rates, 250 rpm and 600 rpm. If we compare the shape of the mean diameter at the lower stirring rate (250 rpm) with agglomeration and without agglomeration (Figure 8), we see no difference. At the higher stirring rate (600 rpm), agglomeration results in a continuous increase in the mean diameter, but it remains constant if no agglomeration is taken into account. In Figure 11 the simulated total number of particles vs. time is plotted. It is important to emphasize that the agreement between experimental and simulated plots is obtained directly (Figures 6b and 11), without any fitting. In particular, these results confirm the low agglomeration efficiency, as predicted by our *a priori* calculations.

In conclusion, agglomeration allows us to explain the evolution of the total number of particles at a low stirring rate. The model is still imperfect, however, because the simulated mean diameter remains constant while it experimentally increases. This discrepancy could be due to the different approximations we introduce in the calculations.

Secondary Nucleation and Breakage Rates. The experimental results show that the mean diameter decreases at the higher stirring rate (600 rpm), with respect to time, and that the total number of particles increases more and more quickly. This behavior cannot be explained with a model of primary nucleation/growth/agglomeration. A source of new crystals is necessary to take the increasing rate of new crystals production into account.

The production of new crystals from parent crystals existing in a supersaturated stirred solution is often inclusively called secondary nucleation (Botsaris, 1976). In fact, a distinction can be made between the ''true'' secondary nucleation, which involves the liquid layer (Tai and Wu, 1992) adjacent to the crystal surface, and other purely mechanical phenomena, such as attrition, fragmentation, or breakage.

We have tested four models of secondary nucleation:

- ''True'' secondary nucleation
- Attrition or erosion
- Breakage into two equal parts
- Breakage into a half part plus two quarter parts.

Table 2. Expression of the Terms B_{II} and B_j in the Expression of the Population Balance

	"True" Secondary Nucleation	Attrition	Breakage in 2 Equal Fragments	Breakage in 3 Unequal Fragments (1/2 + 2×1/4)
B_{II}	$k_2\omega^{b2}M_2(C-C_{eq})^{n2}$	$k_3\omega^{b_3}M_2^1$	$k_3\dot{\gamma}^{1.6}M_3$	$2k_3\dot{\gamma}^{1.6}M_3$
B_j $1\le j\le 6$	0	0	$k_3\dot{\gamma}^{1.6}(2^{1-j/3}-1)M_{3+j}$	$k_3\dot{\gamma}^{1.6}(2^{1-j/3}+2^{1-2j/3}-1)M_{3+j}$

"True" secondary nucleation and attrition both release nuclei of negligible size into the solution. On the other hand, breakage generates crystals with a size comparable to that of the parent crystal.

Solving the model

The method of the moments is applied to solve the problem. The population balance equation (Eq. 5) therefore can be transformed by adding the terms of secondary nucleation to the previous model of primary nucleation/growth/agglomeration. The expression of the moments becomes:

$$\frac{dM_0}{dt} = B_I + B_{II} + A_0$$

$$\frac{dM_j}{dt} = j\cdot G\cdot M_{j-1} + A_j + B_j, \qquad \text{for} \qquad 1\le j\le 6$$

For $j\ge 6$, the system is closed by the relation: $M_j = \overline{R}^{j-5}M_5$. Depending on the nature of the secondary nucleation ("true" secondary nucleation, attrition, breakage), the terms B_{II} and B_j are different (Table 2) and are discussed later.

(1) "True" Secondary Nucleation. For a suspension with a poor concentration of particles (volume fraction $\Phi = 10^{-2}$–10^{-3}), if the former source of nuclei corresponds to true secondary nucleation, the rate of nucleation is expressed as (Botsaris, 1976): $B_{II} = k_2\omega^{b_2}M_2(C_b - C_{eq})^{n_2}$, where k_2 and n_2 are constants. We tested the model, taking $b_2 = 2$ and $n_2 = 1$. We observed the influence of k_2 on the initial mean radius at a stirring rate of 250 rpm. In the absence of secondary nucleation, the initial mean radius is 4.78 μm. This value decreases as the value of k_2 is increased, because the number of particles that is initially formed is greater. Moreover, if the secondary nucleation becomes more active than the primary nucleation, the initial mean radius goes to a value calculated using the relation (Herri, 1996):

$$\overline{R}^3 = \frac{1}{2}\,\frac{\tilde{k}_g}{k_2\omega^2} = \frac{1}{2}\,\frac{1.2+0.06\omega^{0.58}}{k_2\omega^2}. \qquad (24)$$

This value is obtained by rearranging the basic equations of the model and supposing that secondary nucleation is dominant. In this case, the initial mean diameter should be a decreasing function of the stirring rate, because growth rate depends on $\omega^{0.52}$ and the secondary nucleation is proportional to ω^2. Experimentally, we have observed the contrary: the initial mean radius is an increasing function of the stirring rate. To reproduce this experimental behavior using the Eq. 24, we have calculated that the secondary nucleation rate must be proportional to $\omega^{-2.5}$. This means that the secondary nucleation rate should be a decreasing function of the stirring rate which is inconsistent with the common assumptions. As a conclusion, the "true" secondary nucleation cannot have an important role in the crystallization of methane hydrate.

(2) Attrition. For a suspension with a poor concentration of particles, attrition can be expressed as in Table 2. Figures 12 and 13 show that attrition introduces an increase in the rate of nuclei production, which results in a decrease in the mean diameter with respect to time. The higher the value of the attrition constant, the more amplified this behavior becomes. The value of $k_3 = 3\times 10^{-12}$ is the best value reproducing the experimental observations at a stirring rate of 600 rpm.

(3) Breakage into Two Equal Parts. Another source of new particles, which is called breakage in this article, is associated with the crystal production rate. For particles that are smaller in size than the Komolgoroff scale, the rate of breakage is proportional to $\dot{\gamma}^{1.6}$ and proportional to the radius of the particles (M_1/M_0) (Spicer and Pratsinis, 1996). The equations are given on Table 2.

In Figures 14 and 15, we can see the complex effect of breakage coupled with agglomeration. During the first moments of crystallization, breakage gives rise to a behavior comparable to that of attrition: a decrease in the mean diameter with respect to time and an increase in the total number of particles. Further, the higher the k_3 value, the steeper this decrease and the stronger the increase in the total particle number. But after a time, a reversal of this behavior is observed: the mean diameter begins to increase and the total

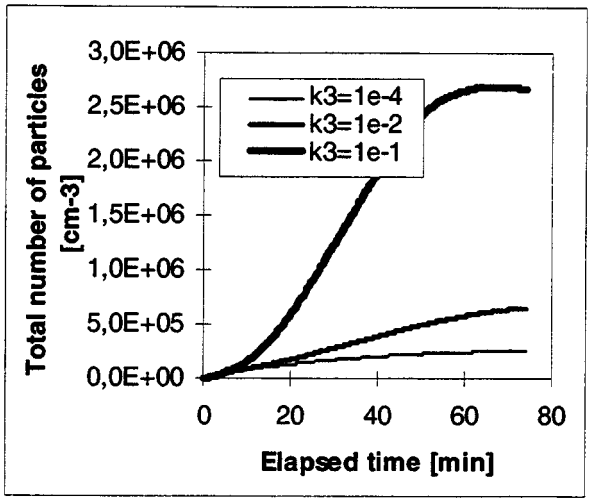

Figure 15. Influence of k_3 (breakage constant) on the total number of particles at a stirring rate of 600 rpm.

number of particles begins to decrease. This is due to agglomeration, which is activated by the increase in the total number of particles. This is not observed in the case of attrition, because the agglomeration constant K is proportional to the cube of the mean diameter. In fact, attrition generates very small particles; this results in a more rapid decrease in the mean diameter than with breakage, which generates crystals of a larger size (comparable to the parent crystal size). As a result, attrition deactivates agglomeration because of the rapid decrease in the agglomeration constant K, while breakage activates it.

(4) Breakage into a Half Part Plus Two Quarter Parts. We have tested a model for breakage into a half part plus two quarter parts (Table 2). Theoretically, this could result in a more rapid decrease in the mean diameter than in the case of breakage into two equal parts, but less rapid than in the case of attrition. We have observed that the consequences of breakage into a half part plus two quarter parts are practically the same as those of breakage into two half parts.

Conclusion on secondary nucleation

Among the different processes of secondary nucleation, we have proved that only the mechanical processes can be retained. In fact, in our model, ''true'' secondary nucleation, which is methane-concentration dependent, results in the dependence of the initial mean diameter with respect to the stirring rate. This is not compatible with experimental observations. Only attrition or breakage have no notable effect on the initial mean diameter. We have also shown that only attrition can be invoked to explain the time dependence of the mean diameter and total number of particles at a high stirring rate. In fact, according to our model, breakage tends to ''activate'' agglomeration; this behavior is not clearly observed in our experiments.

Conclusion

Thanks to a new experimental setup, fitted with a turbidimetric sensor, new results on the formation of the methane hydrate have been obtained. The possibility of determining the *in situ* population-density function provides the crystallization model with new data and makes a better understanding of the mechanisms possible.

We have performed a parametric study of the model in order to determine successively the importance of the different processes in hydrate formation, their main aspects, and to estimate the unknown parameters. In this study, maximum agreement has been sought between the experimental and simulated results concerning particularly $N_T(t)$, $\overline{R}(t)$, and their dependence with respect to stirring rate:

(1) A simplified model of primary nucleation/growth is sufficient to explain the influence of the stirring rate on the initial mean diameter and the initial total number of particles. It is important to point out here that knowledge of the parameters $(k_1,\ B)$ is sufficient to explain the evolution of the initial mean diameter with respect to the stirring rate.

(2) The influence of agglomeration has been tested to explain the evolution of the mean diameter and total number of particles vs. time. It appears that agglomeration does not have much influence at a low stirring rate, which is not sufficient to explain the increase in the mean diameter that is observed experimentally, though it explains very well the shape of the curve representing the time evolution of the total number of particles.

(3) In order to explain the behavior of crystallization at a high stirring rate, we have introduced secondary nucleation. We have tested four models: ''true'' secondary nucleation, attrition, and two types of breakage. It appears that only attrition is able to explain the experimental results.

Thanks to this reactor and to this model, it should be possible in the future to understand which steps of the crystallization process are affected by an inhibitor and to what extent. This could be an interesting method for selecting efficient inhibitors.

Literature Cited

Armenante, P. M., and D. J. Kirwan, ''Mass Transfer to Microparticles in Agitated Systems,'' *Chem. Eng. Sci.*, **44**, 2781 (1989).

Baldi, G., R. Conti, and E. Alaria, ''Complete Suspension of Particles in Mechanically Agitated Vessels—Part I,'' *Chem. Eng. Sci.*, **33**, 21 (1978).

Botsaris, G. D., ''Secondary Nucleation—A Review,'' *Industrial Crystallization*, Plenum, New York, p. 3 (1976).

Bylov, M., and P. Rasmussen, ''Experimental Determination of Refractive Index of Gas Hydrates,'' *Chem. Eng. Sci.*, **52**, 3295 (1997).

Camp, T. R., and P. C. Stein, ''Velocity Gradients and Internal Work in Fluid Motion,'' *J. Boston Soc. Civ. Eng.*, **30**, 219 (1943).

Crawley, G. M., M. Cournil, and D. Di Benedetto, ''Size Analysis of Fine Particle Suspensions by Spectral Turbidimetry: Potential and Limits,'' *Powder Technol.*, **91**, 197 (1997).

De Boer, G. B. J., G. F. M. Hoedemakers, and D. Thoenes, ''Coagulation in Turbulent Flow: Part I,'' *Chem. Eng. Sci.*, **67**, 301 (1989).

Eliçabe, G. E., and L. H. Garcia-Rubio, ''Latex Particle Size Determination from Turbidimetry Using Inversion Techniques,'' *J. Colloid Interface Sci.*, **129**, 192 (1989).

Englezos, P., N. Kalogerakis, P. D. Dholabhai, and P. R. Bishnoï, ''Kinetic of Formation of Methane and Ethane Gas Hydrates,'' *Chem. Eng. Sci.*, **42**, 2647 (1987a).

Englezos, P., N. Kalogerakis, P. D. Dholabhai, and P. R. Bishnoï, ''Kinetic of Gas Hydrate Formation from Mixture of Methane and Ethane,'' *Chem. Eng. Sci.*, **42**, 2659 (1987b).

Gaillard, C., ''Cinétique de Formation de l'Hydrate de Méthane dans une Boucle de Laboratoire,'' PhD Thesis, Institut National Polytechnique de Toulouse, Toulouse, France (1996).

Gregory, J., ''Calculation of Hamaker Constants,'' *Adv. Colloid Interface Sci.*, **2**, 396 (1969).

Herri, J.-M., and F. Gruy, ''Calculation of the Index of Refraction of Pure Hydrate Gas Using a Modified Lorentz-Lorenz Model: Application to Methane Hydrate,'' *Mater. Chem. Phys.*, **42**, 54 (1995).

Herri, J.-M., ''Etude de la Formation de l'Hydrate de Methane par Turbidimetrie in situ,'' PhD Thesis, Université Paris VI, Paris (1996).

Herri, J.-M., F. Gruy, J.-S. Pic, M. Cournil, B. Cingotti, and A. Sinquin, ''Interest of In Situ Turbidimetry for the Characterization of Methane Hydrate Crystallization. Application to the Study of Kinetic Inhibitors,'' *Chem. Eng. Sci.*, **153**, in press (1998).

Higashitani, K., K. Yamauchi, G. Hosokawa, and Y. Matsuno, ''Kinetic Theory of Shear Coagulation for Particles in a Viscous Fluid Y,'' *J. Chem. Eng. Japan*, **15**, 299 (1982).

Higashitani, K., K. Yamauchi, G. Hosokawa, and Y. Matsuno, ''Turbulent Coagulation of Particles Dispersed in a Viscous Fluid,'' *J. Chem. Eng. Japan*, **16**, 299 (1983).

Jones, A. G., J. Hostomsky, and Z. Li, ''On the Effect of Liquid Mixing Rate on Primary Crystal Size During the Gas-Liquid Precipitation of Calcium Carbonate,'' *Chem. Eng. Sci.*, **47**, 3817 (1992).

Kerker, M., *The Scattering of Light and Other Electromagentic Radiation*, Academic Press, New York (1969).

Mehta, V. D., and M. M. Sharma, ''Mass Transfer in Mechanically Agitated Gas-Liquid Contactors,'' *Chem. Eng. Sci.*, **26**, 461 (1971).

Monfort, J. P., and A. Nzihou, ''Light Scattering Kinetics of Cyclopropane Hydrate Growth,'' *J. Cryst. Growth*, **128**, 1182 (1993).
Randolph, A. D., ''A Population Balance for Countable Entities,'' *Can. J. Chem. Eng.*, **42**, 280 (1964).
Randolph, A. D., and M. A. Larson, *Theory of Particulate Processes*, 2nd ed., Academic Press, New York (1988).
Saffman, P. G., and J. S. Turner, ''On the Collision of Drops in Turbulent Clouds,'' *J. Fluid Mech.*, **1**, 16 (1956).
Skovborg, P., and P. Rasmussen, ''A Mass Transport Limited Model for the Growth of Methane and Ethane Gas Hydrates,'' *Chem. Eng. Sci.*, **49**, 1131 (1994).
Sloan, E. D., *Clathrate Hydrates of Natural Gases*, Dekker, New York (1990).
Spicer, P. T., and S. E. Pratsinis, ''Coagulation and Fragmentation: Universal Steady-State Particle-Size Distribution,'' *AIChE J.*, **42**, 1612 (1996).
Sridharan, K., and M. M. Sharma, ''New Systems and Methods for the Measurement of Effective Interfacial Area and Mass Transfer Coefficients in Gas-Liquid Contactors,'' *Chem. Eng. Sci.*, **31**, 767 (1976).
Tai, C. Y., and J. F. Wu, ''Interfacial Supersaturation, Secondary Nucleation, and Crystal Growth,'' *J. of Crystal Growth*, **116**, 294 (1992).
Van de Hulst, H. C., *Light Scattering by Small Particles*, Dover, New York (1957).
Van de Ven, T. G., and S. G. Mason, ''The Microrheology of Colloid Despersions: VII. Orthokinetic Doublet Formation of Spheres,'' *Colloid Poly. Sci.*, **255**, 468 (1977).
Volmer, M., and A. Weber, ''Keimbildung in ubersattigten Gebilden,'' *Z. Phys. Chem.*, **119**, 277 (1926).
Von Smoluchovski, M., ''Versuch einer mathematischen Theorie der Koagulationskinetik Kolloider Lösungen,'' *Z. Phys. Chem.*, **92**, 129 1917).
Vysniauskas, A., and P. R. Bishnoi, ''A Kinetic Study of Methane Hydrate Formation,'' *Chem. Eng. Sci.*, **38**, 1061 (1983).
Vysniauskas, A., and P. R. Bishnoi, ''A Kinetic Study of Ethane Hydrate Formation,'' *Chem. Eng. Sci.*, **40**, 299 (1985).
Wachi, S., and A. G. Jones, ''Mass Transfer with Chemical Reaction and Precipitation,'' *Chem. Eng. Sci.*, **46**, 1027 (1991a).
Wachi, S., and A. G. Jones, ''Effect of Gas-Liquid Mass Transfer on Crystal Size Distribution During the Batch Precipitation of Calcium Carbonate,'' *Chem. Eng. Sci.*, **46**, 3289 (1991b).
Wilke, C. R., and P. Chang ''Correlation of Diffusion Coefficients in Dilute Solution,'' *AIChE J.*, **1**, 264 (1955).
Zettelmoyer, A. C., *Nucleation*, Dekker, New York (1969).

Manuscript received June 9, 1998, and revision received Dec. 22, 1998.